

Contents lists available at ScienceDirect

# **OpenNano**

journal homepage: www.elsevier.com/locate/onano





# Modelling tenofovir release kinetics from hyaluronidase-sensitive nanomedicine: A deterministic approach

Coulibaly S. Fohona a, Vivek Agrahari a, Naveen K. Vaidya b, c, d, Bi-Botti C. Youan a, a

- <sup>a</sup> Laboratory of Future Nanomedicines and Theoretical Chronopharmaceutics, Division of Pharmacology and Pharmaceutical Sciences, School of Pharmacy, University of Missouri—Kansas City, 2464 Charlotte Street, Kansas City, MO 64108, USA
- <sup>b</sup> Department of Mathematics and Statistics, San Diego State University, San Diego, CA 92182, USA
- <sup>c</sup> Computational Science Research Center, San Diego State University, San Diego, CA 92182, USA
- <sup>d</sup> Viral Information Institute, San Diego State University, San Diego, CA 92182, USA

#### ARTICLE INFO

# Keywords: Deterministic approach Mathematical modeling Release kinetics Stimuli sensitive HIV prevention Nanomedicine Nanocarrier

#### ABSTRACT

Despite being convenient and practical, current nanomedicine (NM) release kinetic models remain unscalable, non-specific and less descriptive of the underlying physicochemical determinants. However, a deterministic mathematical modelling could overcome these limitations. In this study, we develop a model, based on a system of two differential equations (accounting for nanoparticle (NP) degradation and then drug release from degraded NM), which enable us to estimate per capita rate constant  $\alpha$  (#NP degraded/hr) and  $\beta$  (Drug Amount Released/NP), the net effect of the nanomedicine (NE factor  $\gamma = \alpha.\beta$ ) and the controlled release index ( $\phi$ , ratio of drug release to NP degradation). The model analysis conducted with tenofovir loaded hyaluronidase sensitive NM clearly shows the  $\alpha$  factor significantly increased with triggering stimuli due to its enzymatic action on its substrate (hyaluronic acid). However, the β factor remained relatively unchanged, due to intrinsic physicochemical properties of the drug as limiting factor. The application of the solutions of this model clearly enabled us to effectively screen among various nanoformulations and identified the best hyaluronidase-sensitive NM formulation, exhibiting the highest ratio (3.7-fold increase compared to no enzyme). The  $\phi$  value confirmed the controlled release and stimuli sensitivity of the nanosystem. Moreover, the computed drug release rate (dM/ dt) is consistent with other existing mathematical models (under valid assumption). The key advantages of this approach are i) relevancy to underlying physicochemical and biochemical process, ii) versatility and application to various NM kinetics, and iii) prediction of temporospatial distribution of the drug loaded NP that could potentially improve in-vitro/in vivo correlation study. This unique approach is applicable for a more specific and more meaningful/ physicochemically relevant description of bioactive agents release from NM or NP for various applications.

# 1. Introduction

HIV still remains one of the biggest public health concerns in the world. Despite tremendous success of controlling viral infection through antiretroviral therapies, there is no cure for HIV. Moreover, efficient HIV vaccines have not yet been developed. In the absence

E-mail address: youanb@umkc.edu (B.-B.C. Youan).

https://doi.org/10.1016/j.onano.2023.100167

<sup>\*</sup> Corresponding author.

of HIV vaccines, strategies, such as delivering microbicide that destroy HIV or prevent its entry in the vaginal mucus, have been considered for potential HIV prevention. Among these strategies, nanoparticle-based treatment in vagina mucus has received much attention [1–4]. Therefore, understanding the distribution of nanoparticles (NPs) or nanomedicines (NM) in the vaginal mucus and drug-release mechanism are critical for implementation of such drug-loaded NPs for practical purposes.

Mucus, a viscoelastic coating fluid is present in the eye, the gastrointestinal tract, the respiratory tract, and the female reproductive tract [5,6]. Its known purposes are a protective action of underlying epithelium by surface lubrication and foreign particles entrapment and removal [7,8]. To escape this barrier, drug delivery system may be designed to penetrate through the mucus layer at a rate faster than the mucus renewal cycle [5]. Few strategies have been proposed to avoid the mucus barrier when reaching the epithelium. Among these strategies, high density pegylation of NPs remains one of the most studied and proven successful [5,9,10]. However, owing to the diversity in delivery strategies, pegylation is not always an appropriate approach. Indeed, with the increasing interest in nanomedicine research, new delivery strategies are being constantly explored. This often implies the use of new and complex coating, targeting and stimuli sensitive systems.

Taking advantage of Hyaluronidase (HAase), an abundant enzyme found in human seminal fluid and several body fluids and tissue [11,12], we previously developed (HAase)-sensitive NPs (HA-NP) templates for HIV/AIDS microbicide triggered release *in vitro* [13]. HA-NP was engineered and intended for the potential prevention of HIV/AIDS and other sexually transmitted diseases. HA-NP were stable, spherical in shape and non-cytotoxic (MTT assay) to human vaginal cells (VK2/E6E7 and End1/E6E7) and *Lactobacillus crispatus*. Furthermore, HAase was found to trigger HA-NP degradation with a significant drug release compared to control experiments without enzyme [13]. While these studies indicated the potential for using HA-NP as an efficient means of HIV drugs through vagina mucus, its mass transport and release mechanism has not been fully evaluated.

Mass transport and release has been proven to be critical factors in the design, application and approval of novel drug delivery systems [14–16]. Analysis of mass transport becomes more important when the medium is proven to be constantly renewing, as for vaginal mucus. Indeed, depending on the anatomical organ, mucus turnover varies between seconds to few hours [7,17], implying a real challenge for drug delivery systems designed to interact with a mucus layer as they could significantly be cleared. While most traditional drug release studies approximate the release of an active agent from a carrier [18,19], those techniques however rarely considered the transport of the carrier itself [20,21], which can dramatically impact the overall drug transport, release profile, and performance of the proposed system. In reality, the overall transport of a drug from a drug nanocarrier system can be considered as a combination of two major phases, one involving the transport of the loaded nanocarrier and the release of the drug from the nanocarrier. Thus, studying both the drug mass transport as well as distribution of the nanocarrier systems in their intended delivery medium are critical to properly evaluate and elucidate the potential advantages or limitations of the delivery strategy.

Computational and mathematical modeling and simulation studies, together with bench, nonclinical *in vivo*, and clinical studies, can be used to evaluate the safety and effectiveness of the drug delivery systems. In this study, we use mathematical models to investigate Tenofovir (TFV) loaded HA-NP mass transport in vaginal mucus. Using these models, we identify the spatio-temporal dynamics of TFV loaded HA-NP, and compute the time and amount of HA-NP that can cross various mediums such as water, vaginal fluids and vaginal-seminal fluids. In addition our model allows us to estimate per capita rate constant  $\alpha$  (#NP/hr) and  $\beta$  (# Drug Amount Released/NP), the net effect of the nanomedicine (NE factor  $\gamma = \alpha.\beta$ ) and the controlled index ( $\phi$ , ratio of drug release to NP degradation). This study will not only extend our understanding of HA-NP vaginal distribution, but the results obtained could also be applied to other nanocarrier based drug delivery systems.

#### 2. Material and method

Hyaluronic acid sodium salt (MW, 11,624 Da) was supplied by Zhenjiang DongYuan Biotech Co., Ltd., (Jiangsu, China). Tenofovir (99% purity) was purchased from Beijing Zhongshuo Pharmaceutical Technology Development Co. Ltd. (Beijing, China). The following reagents; Hyaluronidase (HAase) from bovine testes with a specified activity of 810 U/mg, bovine serum albumin (BSA, Fraction V), adipic acid dihydrazide (ADH), *N*-hydroxysuccinimide (NHS), acetone and sodium d-glucuronate were purchased from Sigma-Aldrich (St. Louis, MO, USA). 1-Ethyl-3-[3-dimethylaminopropyl] carbodiimide hydrochloride (EDC) was from Thermo Fisher Scientific Inc. (Rockford, IL, USA). Dialysis bag (Spectra/Por Float-A-Lyzer G2, MW-CO, 3.5–5 kDa) were supplied from Spectrum Laboratories Inc. (Rancho Dominguez, CA, USA).

Formulation of TFV loaded HA-NP. HA-NP formulation was prepared through the surfactant-free cross-linking method previously reported in Agrahari et al. [13] Briefly, to ten milliliters (10 mL) of HA aqueous solution (1 mg/mL), acetone was added at a ratio of 40%v/v under constant agitation. After stirring for an hour (1 h), 250  $\mu$ L of EDC, NHS, and ADH (concentration ranging from 2.49 to 9.96 mM)) were respectively added to the above solution and the mixture was stirred for 30 min, after each addition. The carbodiimide mediated cross-linking reaction, leading to the formation of amide bonds between the carboxylic acid groups of glucuronic acid units of HA and the hydrazide groups of ADH, was further continued at room temperature for 15 h under agitation. After cross-linking reaction completion, which was monitored by Fourier Transform InfraRed spectroscopy (FTIR- Nicolet iS10 Spectrometer, Thermo Scientific, West Palm Beach, FL, USA) and solid state  $^{13}$ C nuclear magnetic resonance (NMR Tecmag Apollo console, Houston, TX, USA), the organic solvent was evaporated by rotary evaporation (BUCHI Labortechnik AG, Flawil, Switzerland). From the resulting colloidal dispersion, HA-NP were isolated by ultra-centrifugation on a Beckman L8–70 M ultra-centrifuge (Beckman Instruments Inc., Palo Alto, CA, USA) at 20,000 rpm and 10 °C for 45 min. HA-NP were further purified by dialysis against 1 L of DI water for 24 h, and freeze-dried overnight (Labconco Corporation, Kansas City, MO, USA).

Subsequently, TFV was encapsulated in HA-NP through the soaking method. Typically, 10 mg of purified and freeze-dried HA-NP were immersed in an aqueous solution (pH 7) of TFV (10 mg) at room temperature for 3 days. TFV percent encapsulation efficiency (%

EE) and drug loading (%DL) in HA-NP were determined indirectly from the supernatant using a high-performance liquid chromatography (HPLC) assay [22].

# 2.1. Size and zeta potential measurement

HA-NP average particle size and apparent zeta potential ( $\zeta$ -potential) were measured on Malvern instrument 3600 Zetasizer Nano (Worcestershire, UK) [23]. Practically, 1 mL of nanoparticle suspension was prepared in appropriate solvents [DI water, vaginal fluid simulant (VFS), vaginal and seminal fluid simulant mixture (VFS/SFS; 1:4 (v/v))] and sonicated (Qsonica LLC, Newtown, CT, USA) for 10–20 s. Prior to sample preparation, all solvents were filtered on a 0.2  $\mu$ m Whatman PTFE syringe filter (Fisher Scientific, Waltham, MA, USA). Following the sonication, the sample was immediately placed in the measurement cuvettes and the experiment was performed at 25 °C. The sample was allowed to equilibrate in the zetasizer instrument for 1 min before data acquisition. All data acquisition and analysis were conducted using Zetasizer software (version 6.01, Worcestershire, UK). VFS (pH 4.37) and SFS (pH 7.5) were prepared according to the method of Owen et al. [24,25].

# 2.2. Morphological analysis

HA-NP morphology was imaged by transmission electron microscopy (TEM). Briefly, few drops ( $\sim 10~\mu L$ ) of HA-NP sample (in DI water) were placed onto a carbon-coated copper grid support. The sample is then dried at room temperature. TEM images were captured on Philips TEM C12 instrument (FEI, Hillsboro, OR, USA) equipped with a large format (II Megapixel), retractable and fiberoptical coupled SC100 ORIUS $_{\odot}$  CCD camera (Gatan, Inc., Pleasanton, CA, USA). The TEM observations were performed at an accelerating voltage of 80 kV. [26]

# 2.3. Assessment of tenofovir release by high performance liquid chromatography

TFV release from HA-NP was investigated in the presence of the bovine testicular Hyaluronidase (HAase) [13]. Briefly, 10 mg of TFV loaded HA-NP was dispersed in 3 mL of VFS/SFS mixture (1v/4v) containing 1.08 U of HAase enzyme. The dispersion was then transferred into a dialysis bag submerged into a dialysis tube containing 20 mL of VFS/SFS mixture. The release was performed at 37 °C in a thermostatic shaking water bath (BS-06, Lab Companion, Seoul, Korea) at 60 rpm. Hundred microliters ( $100 \mu L$ ) from the dialysis tube were collected at 0, 1, 3, 6, 9, 12, 24, 48, and 72 h and the amount of TFV released is quantified using a previously published HPLC method [22]. Briefly, the HPLC assay was performed isocratically at ambient temperature (23 °C) using a Bridge<sup>TM</sup> C18 column ( $150 \times 4.6 \text{ mm}$ , 5 µm) as stationary phase. The mobile phase typically consisting of water–methanol was degassed in an ultrasonic bath (Sonicator VWR model 150 D; VWR International., West Chester, PA) for 10 min before their use. The sample volume of  $10 \mu L$  was injected for each run and detected at a wavelength of 259 nm. The drug retention time was  $1.54 \pm 0.03 \min (n = 6)$ . The assay was linear (over the concentration range of  $0.1 - 10 \mu g/ml$ ) and sensitive with LOD and LOQ values equal to 50 and 100 ng/mL, respectively. The method was accurate (percent mean recovery range: 95.41% - 102.90%) and precise (percent relative standard deviation values for intra-day, and inter-day precision < 2%). To maintain the sink condition throughout the duration of the study,  $100 \mu L$  of free VFS/SFS mixture was added to dialysis tube immediately after each sample collection.

# 2.4. Assessment of nanoparticle degradation

As we previously reported [27], an uronic acid–carbazole assay [28] was used to analyze the degradation of the HA-NPs under the influence of HAase enzyme. Briefly, the HA-NPs (10 mg) were dispersed in 3 mL of the simulant mixture (pH 7.1) of vaginal fluid simulant (VFS, pH 4.2) and seminal fluid simulant (SFS, pH 7.8). These VFS and SFS buffers were prepared according to the previous reports [29,30]. The 1:4 ratios of the VFS and SFS, respectively, were used for preparing the simulant mixture, considering the volumes of normal human vaginal fluid and male ejaculate, respectively [27]. The pH of simulant buffers was adjusted using 1 M HCl or NaOH solutions, prepared accordingly. The NPs dispersion was transferred to a dialysis bag (Spectra/Por Float-A-Lyzer G2, MW-CO, 3.5-5 kDa), supplied from Spectrum Laboratories Inc. (Rancho Dominguez, CA, USA), and placed inside a dialysis tube containing 20 mL of the simulant mixture. The whole system was then placed in a thermostatic shaking water bath (BS-06, Lab Companion, Seoul, Korea) with 60 rpm at 37 °C. Aliquots of 100 μL solutions were taken from the medium at different time intervals (0, 1, 3, 6, 24, 48, 72, 96, 120 h), boiled for 10 min to inactivate the enzyme and analyzed for the amount of glucuronic acid released. Simultaneously, the fresh simulant mixture was added at the same rate to maintain the sink condition. The Genesys 10 Bio UV-Vis Spectrophotometer (Thermo Electron Sci. Inst., LLC, Madison, WI, USA) was used for the degradation analysis at 530 nm. The amount of glucuronic acid released at each time point was determined by using the standard curve of sodium p-glucuronate. The curve was found linear in the concentration range of 0–200  $\mu$ g/mL (square of the correlation coefficient:  $r_2$ =0.99). The measured amount of p-glucuronic acid was represented as percent cumulative degradation (%w/w) of NPs compared to the degradation of native HA incubated either in the presence or absence of HAase.

# 2.5. Viscosity measurement

Deionized (DI) water, VFS and VFS/SFS viscosity was measured using a Cannon-Fenske viscometer tube size 50 (Sigma-Aldrich, St. Louis, MO, USA) [31]. Briefly, 10 ml of blank solvents are placed into a clean viscometer and a suction is applied to raise the sample to

the top mark line. The time taken by the solvent to go from the top mark to the bottom mark line is recorded in second. Experiments are run in triplicates and the average time is determined. The kinematic viscosity  $(mm^2/s (Cst))$  is then computed using Eq. (1).

$$\nu = C \times \theta,\tag{1}$$

where  $\nu$ , C and  $\theta$  represent the kinematic viscosity, the viscometer constant and the average time, respectively. For Cannon-Fenske viscometer tube size 50 the constant  $C=0.004~\text{mm}^2/\text{s}$  or 0.004 cSt. The dynamic viscosity (in cP) may be obtained by multiplying the kinematic viscosity (in cSt) x density..

# 2.6. Refractive index measurement

DI water, VFS and VFS/SFS refractive index was measured on Leica Auto Abbe refractometer. Prior to any measurement, the prism was thoroughly cleaned with DI water and ethanol and the equipment was calibrated using DI water. Typically, experiment is conducted by covering the prism' surface with the sample and allowing 2 min of contact, for equilibration. When properly calibrated, the instrument shows typical refractive index values between 1.3332 and 1.3319, for DI water.

# 2.7. Diffusion coefficient measurement

HA-NP diffusion coefficient in water, VFS and VFS/SFS was determined from the Stokes-Einstein equation following size measurement. Practically, new dispersant (solvent) specifications were customized in Zetasizer software' dispersant manager tool using VFS and VFS/SFS viscosity and refractive index values, previously determined as explained above. Then particle size measurement was conducted at 25 °C by Dynamic Light Scattering (DLS) on Malvern instrument.

From the Einstein-Smoluchowski [32,33], we have

$$D = \mu k_B T, \tag{2}$$

where D is the diffusion constant,  $\mu$  is the mobility,  $k_B$  is the Boltzmann's constant and T is the absolute temperature expressed in kelvin (K). Using the mobility  $\mu$  as the inverse of the drag coefficient  $\xi$  for liquids with low Reynold number, i.e.  $\mu = \frac{1}{\xi}$ , and the Stokes' law  $\xi = 6\pi\eta r$ , we obtain the Stokes-Einstein's equation

$$D = \frac{k_B T}{6\pi \eta r},\tag{3}$$

where  $\eta$  represents the dynamic viscosity of the medium and r is the radius of the spherical nanoparticles.

The validity of DLS approximation of particle translational diffusion coefficient based on Stokes-Einstein's equation (Eq. (3)) has been established by numerous studies [34–36].

# 2.8. Modeling the spatio-temporal distribution of HA-NP

To model the experimental setting, we consider a tube of unit cross section area so that nanoparticle concentration can be measured as per unit length of tube. We use the diffusion driven movement to model the distribution of HA-NP. We assume that C(x, t) is a concentration of nanoparticles at time t and location x. In one dimensional media  $0 \le x \le L$ , the spatio-temporal dynamics of NPs with media-related diffusion coefficient  $D_n$  is governed by the Eq. (4) below [37–39].

$$\frac{\partial C}{\partial t} = D_n \frac{\partial^2 C}{\partial x^2}, \quad 0 < x < L, \ t \ge 0,$$
(4)

 $C(x,0) = 0, \quad 0 < x < L,$ 

 $C(0,t)=C_{\infty}, \quad t\geq 0,$ 

 $C(L,t) = 0, t \ge 0.$ 

Here, L represents the length of the media and  $C_{\infty}$  represents the concentration of the constant source of HA-NPs introduced into the media at the boundary x = 0. Note that we assumed the HA-NPs that arrived at another boundary x = L, do not get accumulated at the boundary and are removed immediately, implying C(L, t) = 0.

# 2.9. Modeling the release kinetics of TFV from HA-NP

In this experimental setting (see above description), we assume that the HA-NPs degrade with a per capita rate of  $\alpha$  per hour and the degraded HA-NPs release drug at a rate of  $\beta$  amount of drug per NP. With these rates, the number of HA-NPs and the amount of drug released, M(t), are given by the following system of differential equations.

$$\frac{dN_T}{dt} = -\alpha N_T, \ N_T(0) = N_{T0},$$
 (5)

$$\frac{dM}{dt} = \beta \alpha N_T, \quad M(0) = M_0, \tag{6}$$

where  $M_0$  is the initial amount of drug released and  $N_{T0}$  is the initial number of HA-NPs in the dialysis bag.

#### 2.10. Determination of initial model parameters relevant to the experimental condition

Using the formula  $N = 6/\pi d^3 \rho$ , where d is particle mean diameter and  $\rho$ , the particle density, we estimated that the initial number of particles in the 10 mg of formulation ( $N_{T0}$ ) to be  $4.25 \times 10^{13}$ ,  $2.33 \times 10^{13}$ , and  $3.35 \times 10^{12}$  for formulations F13 (d= 70.6 nm), F1 (d= 81.5 nm) and F7 (d= 157.7 nm), respectively. Based on literature the density of HA-NP is assumed to be 1 g/cm<sup>3</sup> [40]. Considering the respective weight percent drug loadings of 26.1%, 22% and 10.6%, for F13, F1 and F7, and total amount of solvent in the release media (23 mL), the  $C_{\infty}$  (drug concentration after completion of 100% release) was estimated to be 113.48, 95.65, and 46.08 µg/mL for F13, F1 and F7, respectively. Considering drug loading and nanoparticle number, the initial drug loading per nanoparticle (beta zero) for each formulation is 0.04, 0.06, and 0.24 femtogram (fg) for F13, F1, and F1, respectively.

# 2.10.1. Data analysis

A multi-factorial statistically analysis was conducted to assess the significance at alpha level = 0.05 of the variance of these measurements between the different groups using Microsoft Excel 365. Pairwise comparisons between the two factors were examined to determine which factors groupings were significant. The null hypothesis  $H_0$  and alternative hypothesis  $H_1$  were as follows: the measurements (e.g. viscosity, mean diameter, charge density, diffusion coefficient) of each factor grouping are the same and not all these measurements of each factor grouping are the same, respectively.

#### 3. Result and discussion

Characteristics of TFV loaded HA-NPs. The encapsulation efficiency, and drug loading of these HA-NPs were  $51.8 \pm 2.4\%$  w/w and  $26.1 \pm 1.2\%$  w/w, respectively, (n = 3). We have previously published TEM of these nanoparticles showing greater number of particles [27]. This manuscript focuses on the mathematical modeling aspects of that study. The readers are encouraged to refer to that published manuscript for additional morphological information. The additional TEM imaging of TFV loaded HA-NP in DI water (Fig. 1A) showed the spherical morphology of the nanomicrobicide with average particle size around 100 nm (n = 5), as confirmed by

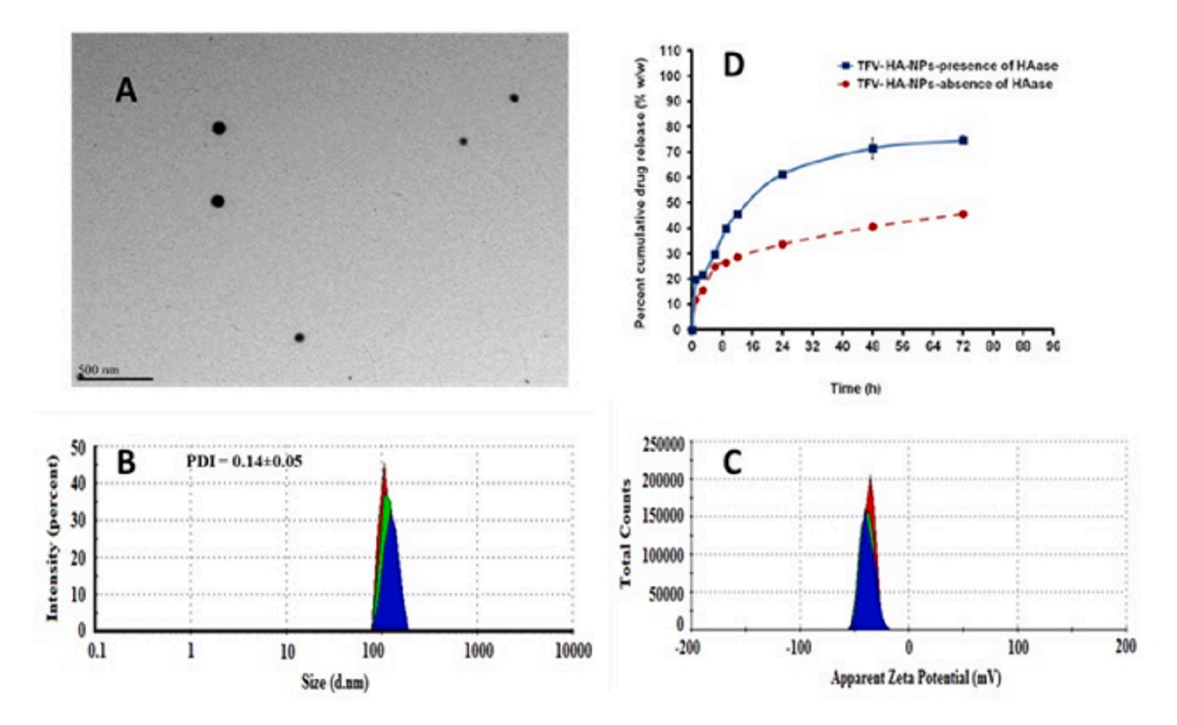


Fig. 1. HA-NP TEM image (A), average particle size (B), apparent zeta potential (C) determined in DI water. TFV release profile from HA-NP in the presence and absence of HAase is presented in D. Fig. 1D was reproduced from Agrahari et al.(13) with permission from the AAPS journal. Scale bar represents 500 nm.

particle size distribution (Fig. 1B). In fact, the average particle size measured by DLS was found to be  $106.2 \pm 11.53$  nm (n = 3) in DI water, and the polydispersity index (PDI) of  $0.14 \pm 0.05$  (Fig. 1B). HA-NP  $\zeta$ -potential, indicative of the surface charge, was  $-37.7 \pm 1.12$  mV (n = 3) in DI water (pH 7.1) (Fig. 1C). The strong negative charge observed in DI water could be due, in part, to the carboxylic acid group of Hyaluronic acid (HA), which has a pKa value of 2.59 to 3 [41,42], and is therefore expected to be negatively charged at pH 7.1. Furthermore, Tenofovir (TFV), a weak acid has two pKa values of 3.8 and 6.7 and would also be expected to be negatively charged in DI water at pH 7.1 and thus contributing to the NPs negative charge density [41].

Characteristics of the release media. Table 1 shows physico-chemical parameters determined for three different release media: water, VFS and VFS/SFS mixture. Although VFS/SFS mixture had a slightly higher refractive index, no significant difference between the refractive index of water and that of VFS was noticeable at 25 °C. Nonetheless, the trend observed in the refractive index measurement was consistent with the viscosity results. Statistical analysis of the viscosity data (Table 1) shows that the tested samples exhibited different viscosities (the lowest was that of DI water and the highest was that of the mixture of VFS/SFS due to its more complex composition resulting in stronger intermolecular interaction and resistance to flow). Several studies have established a linear relationship between the refractive index and viscosity for a given fluid. In fact, it is generally accepted that the refractive index of a fluid increases as its viscosity increases [42,43] as a linear relationship (Eq. (7)) established by Lagemann between the molecular refraction R (refractive index) and the viscosity constant (n) (expressed as Souder's index I) for a given fluid.

$$I = aR + b \tag{7}$$

$$I = \frac{Mol}{d}(log_{10}(log_{10}\eta) + 2.9)$$
(8)

In Eqs. (7) and (8), Lagemann' constants a and b are specific to a given fluid while Mol and d are the fluid' molar mass and density, respectively.

Interaction of HA-NPs and the media. The viscosity and refractive index values were set as parameters in DLS size and  $\zeta$ -potential measurement for the respective fluids. As shown in Table 2, HA-NP average size increased in VFS (150.4  $\pm$  7.85 nm) and VFS/SFS  $(113.27 \pm 8.46 \text{ nm})$  mixture. The apparent increase in particle average size could be due, in part, to bovine serum albumin (BSA) adhesion onto HA-NP surface as well as charge-charge interactions between the negatively charged HA-NP and other positively charged components present in VFS and VFS/SFS. Such interactions could lead to media material adhesion onto HA-NP nanoparticle surface. In fact, one of the major biological components of VSF and SFS is bovine serum albumin (BSA). In the present study, VFS and SFS were prepared at BSA concentrations of 0.018 g/L and 50.4 g/L, respectively, according to the method of Owen et al. [24,25] Several studies have shown that BSA isoelectric point (PI) varies between 4.7 and 5.2 [44-46]. That is, below these PI values, BSA is positively charged (due to predominant protonation of its amino groups) and the protein is negatively charged (due to predominant deprotonation of its acidic groups) above these PI values [47]. In VFS, where the pH (4.37) is below the BSA's PI value and above HA polymer's carboxylic acid pKa value (2.59 to 3), electrostatic attraction between positively charged BSA and negatively charged HA-NP is probably responsible for the average size increase observed. This phenomenon was previously described by Boulos et al. with positively charged polyallylamine hydrochloride coated gold nanoparticles [48]. HA-NP average size increase was also observed in VFS/SFS mixture, despite the negative charge of both HA-NP and BSA. Numerous studies have also established the ability of BSA to adhere onto surfaces regardless of their charged state. In fact, Jachimska et al. showed that BSA adsorbed and formed a monolayer onto negatively charged fluorescent latex nanoparticles at pH values above its PI (pH 5.7, 6.5 and 10) [29]. Similar observations were also reported by Boulos et al. when sodium poly(acrylic acid) functionalized gold nanoparticles were exposed to BSA above its PI value [48]. Furthermore, using a quartz crystal microbalance approach, Phan et al. demonstrated BSA binding onto negatively charged Mercaptoundecanoic acid (MUA) surface above the protein's PI value [30]. BSA binding onto negative surfaces at pH values above its PI was attributed to electrostatic interactions with positively charged amino acid residues in the protein structure [49,50]. The adsorption of BSA onto HA-NP in VFS and VFS/SFS could potentially explain the substantial decrease in the apparent ζ-potential observed in those fluids (Table 2). The statistical analysis showed that although the diameter and charge data were statistically different between VFS and VFS/SFS. There was no statitically significant difference in the HA-NPs diffusion data. This obervation is mainly ascribed to the significant difference in these two media viscosities. Considering the above Stokes-Einstein Eq. (3), the net diffusion effect of larger HA-NPs in a relatively lower viscosity media (VFS) appear similar to that of relatively smaller particles in the more viscous media (VFS/SFS mixture). However, the diffusion coefficient in DI water was statitiscally significantly higher due to the lowest particle size and water viscosity.

Diffusion coefficient of HA-NP. As expected from the Stokes-Einstein's equation, the calculated diffusion coefficients values were inversely proportional to HA-NP average size. Therefore, as HA-NP average size increased from one fluid to the other with both of them having similar viscosity (Table 1), the corresponding translational diffusion coefficient values decreased accordingly. We observed that

**Table 1**Physico-chemical parameters of dispersion medium.

Parameters	DI Water	VFS	VFS/SFS
Refractive index (R)	1.3328	1.33397	1.34352
Viscosityt (cSt)	$\textit{0.95388} \pm \textit{0.004}$	$0.96316 \pm 0.004$ (*)	$1.17 \pm 0.024$ (*)
pH	7.10	4.37	7.08

Note: \* Statistically significant compared to DI water data (p < 0.05). NS: Not statistically significant compared to DI water data (p > 0.05). These viscosity data were also statistically different between VFS and VFS/SFS.

**Table 2** HA-NP properties in selected dispersion medium.

Fluid	HA-NP average particle $\emph{diameter} \pm SD$ (nm)	HA-NP zeta potential (mV)	HA-NP Diffusion from Stokes equation ( $10^{-8} \text{ cm}^2/\text{s}$ )
VFS	150.4 ± 7.85 (*)	$-20.0 \pm 1.46$ (*)	3.0137 ± 0.5774 (*)
VFS/SFS	$113.27 \pm 8.46$ (NS)	$-12.7 \pm 1.12$ (*)	$3.2941 \pm 0.4411$ (*)
DI water	$106.2 \pm 11.53$	$-37.7\pm1.12$	$4.3095 \pm 0.3969$

Note: \* Statistically significant compared to DI water data (p < 0.05). NS: Not statistically significant compared to DI water data (p > 0.05). Diameter and charge data were statistically different between VFS and VFS/SFS data but NS for diffusion data.

HA-NP has the fastest diffusion rate in water (4.3095  $\times$  10<sup>-8</sup> cm<sup>2</sup>/s) (Table 2). Although VFS/SFS was found to be more viscous than VFS, HA-NP diffusion was slightly higher in VFS/SFS than in VFS alone, showing that the difference in HA-NP size in these fluids is the dominant factor for determining diffusion coefficients. It is noteworthy that the difference in diffusion coefficient and thus transport may also translate into differences in drug bioavailability and therapeutic outcome. That is, the rate of HA-NP vaginal clearance, due to the vaginal fluid renewal cycle in women, could potentially result in differences in TFV bioavailability at the interface of CD4+ target T-cells.

Distribution of HA-NPs in the media. We simulated model Eq. (4) numerically [38] to observe the spatio-temporal distribution of HA-NPs in different medias. For the computation purpose, we took the tube of length L=0.1 cm. Using calculated diffusion coefficients (Table 2) and the source  $C_{\infty}=10^5$  HA-NPs per mL, we obtained the spatial distribution of HA-NPs across different medias in 10, 20, 30 min (Fig. 2). As expected, HA-NPs diffuse farther from the source for a longer time-period. At each time point, the concentration of HA-NPs monotonically decreases from the source to a location away from the source. Also, at each time-point, the concentration of HA-NPs is lower in VFS and VFS/SFS than in water. For example, in 20 mins, the concentration of HA-NPs at x=0.02 cm from the source is 1893, 2480, and 4950 HA-NPs/mL in VFS, VFS/SFS, and water, respectively (Fig. 3). With these diffusion driven movements, at each location, less nanoparticles are available in VFS and VFS/SFS media compared to water (Fig. 3). The actual concentration of HA-NPs that are available at targeted site depends upon the initial NPs concentration at the source as well (Fig. 3). For example, in one hour 162, 54, 35 HA-NPs/mL are available at location x=0.05 cm in water, VFS, VFS/SFS, respectively, when the source is 5 log<sub>10</sub>, while only 16, 5 and 3 HA-NPs/mL, respectively, are available when the source is 4 log<sub>10</sub> (Fig. 4).

*Transit time of HA-NPs across the media.* For evaluation of nanoparticle based preventive therapy, the transit time, the average time nanoparticles take to cross the mucus, is important. Here, we use a mathematical model to calculate the average time for HA-NPs to cross the different medias of length L [37,51]. In a long run, the system eventually reaches the steady state. The steady state solution of the model (4) is given by  $\frac{\partial^2 C}{\partial x^2} = 0$ ,  $C(0) = C_{\infty}$ , C(L) = 0, which provides the solution  $C(x) = C_{\infty} \left(1 - \frac{x}{l}\right)$ . The flux is therefore  $J = -\frac{x}{l}$ 

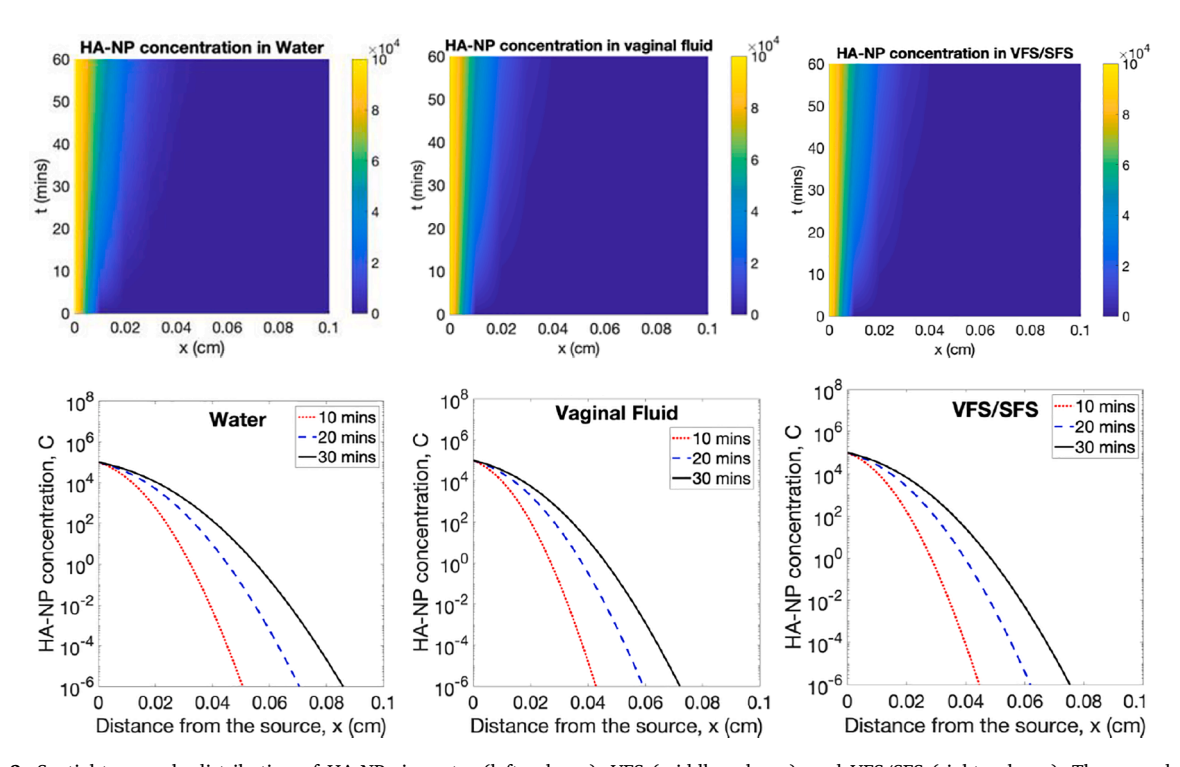


Fig. 2. Spatial-temporal distribution of HA-NPs in water (left column), VFS (middle column), and VFS/SFS (right column). The second row represents the spatial distribution at three different time points (10, 20, 30 mins). These curves were obtained using Eq. (4) and different diffusion coefficients shown in Table 2 for each media.

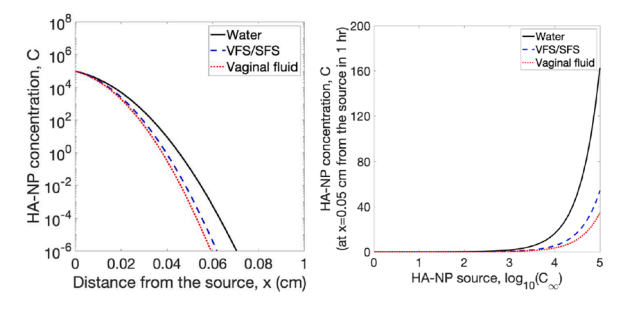


Fig. 3. (Left) Spatial distribution of HA-NPs in 20 mins in different media. (Right) Concentration of HA-NPs at x=0.5 mm from the source in 1 hr for different level of nanoparticle source  $C_{\infty}$  Vaginal fluid simulant is VFS.

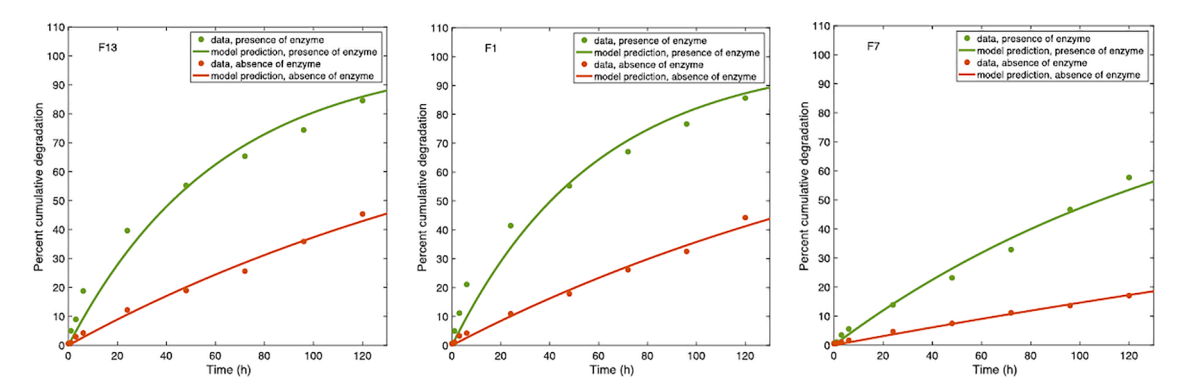


Fig. 4. Prediction of the model (Eq. (9)) (solid line) along with the experimental data (filled circle) of the degradated HA-NPs in the presence (green color) and the absence (red color) of HAase enzyme as function of time.

 $D_n rac{\partial C}{\partial x} = D_n C_\infty / L$ , and hence the diffusion current is  $I = J = D_n C_\infty / L$ . The total number of HA-NPs in the tube of unit cross-section area (media) is given by  $N_T = \int\limits_{-L}^{L} C(x) dx = C_\infty L/2$ . Therefore, the transit time,  $\tau$ , from 0 to L is  $\tau = rac{N_T}{I} = L^2/2D_n$ .

We found that the transit time for HA-NPs to cross the tube of length 0.1 cm an estimation of human vaginal mucus thickness is 32.22 hrs, 46.14 hrs, and 42.22 hrs, in water, VFS and VFS/SFS, respectively. Therefore, HA-NPs tend to stay significantly longer in VFS due to slower movement of HA-NPs in VF, indicating the benefits of using these HA-NPs for the longer time availability in VFS. We note that in physiological conditions and actual vagina mucosa thickness, the conditions are constantly renewed overtime posing some delivery challenges. Our equation with accurate parameters measured from the actual vagina sites might be useful in screening the optimal formulation for effective microbicide delivery.

TFV releases from the HA-NPs. Our group previously investigated mechanism of TFV release from HA-NP in the presence of HAase in VFS/SFS [27] using Korsmeyer–Peppas kinetic model,  $M_t/M_\infty = Kt^n$ , where  $M_t$  and  $M_\infty$  represent the amount of drug release at time t and the total amount of drug, respectively, K is a kinetic constant and n is the exponent parameter explaining the drug release mechanisms [52]. We found that TFV releases from HA-NP through Fickian diffusion mechanism, and that the overall amount of drug released from HA-NP is significantly higher in the presence of HAase enzyme. This difference in drug release could be due to a greater enzymatic degradation of HA-NP in the presence of HAase.

Here, we use our model to further analyze the kinetic process by estimating rates of HA-NPs degradation and drug release per HA-NP, and study how the presence of HAase affects these rates. During the process of dispersion of TFV loaded HA-NPs in VFS/SFS media, the HA-NPs distribution reaches the steady state in a dialysis bag before the drug release was performed. As derived above using diffusion model, the total number of HA-NPs in the test tube (media) at the steady state is given by  $C_{\infty}L/2$ . Therefore, we take the initial number of HA-NPs in the dialysis bag as  $N_T(0) = C_{\infty}L/2$ .

Solving Eq. (5), the HA-NPs remaining in the dialysis bag (i.e., undegraded) is given by  $N_T(t) = N_T(0)e^{-\alpha t}$ . Therefore, the HA-NP degradation rate (the percentage degraded) over time is given by

$$NP_{Deg} = \frac{N_T(0) - N_T(t)}{N_T(0)} \times 100\% = (1 - e^{-at}) \times 100\%.$$
(9)

Where  $\alpha$  represents the drug nanocarrier degradation rate constant or the number of individual/single nanocarrier (or NP) degraded per hour (#NP/hr).

Using  $N_T(t) = N_T(0)e^{-\alpha t}$  in Eq. (6) and solving with  $M_0 = 0$  as no drug was released at the beginning, we obtain the amount of drug

released as  $M(t) = \beta C_{\infty} L/2(1 - e^{-\alpha t})$ . Again, representing the total amount of drug as  $M_{\infty}$ , the drug release rate (the percentage cumulative drug released over time) is given by

$$Drug_{Rel} = \frac{M(t)}{M_{\infty}} \times 100\% = \frac{\beta LC_{\infty}}{2M_{\infty}} (1 - e^{-at}) \times 100\%.$$
 (10)

Combining Eqs. (9) and (10), we obtain

$$Drug_{Rel} = \varphi NP_{Deg}, \tag{11}$$

where  $\varphi = \frac{\beta L C_{\infty}}{2M_{\infty}}$  that can be regarded as the drug-controlled release index and  $\beta$  is the rate of drug release per individual/single nanocarrier or NP (# Drug Amount Released/NP),

As above, we consider L=0.1 cm. From Agrahari et al. [27], the ratio of HA-NPs to drug amount in the loading solution was varied from 10:1 to 1:1. This helps us to estimate  $C_{\infty}/M_{\infty}$  to lie between 1 and 10. Therefore, for our base case computation, we use  $\frac{C_{\infty}}{M_{\infty}}=5:1$ . We fitted the curve given by Eq. (9) to HA-NP degradation data and estimated the per hour rate of HA-NP degradation,  $\alpha$ . We also performed curve fitting for linear relation given by Eq. (11) to drug releases versus HA-NP degradation data to estimate the slope or the drug-controlled release index  $\varphi$ . The value of  $\varphi$  was then used to calculate the rate of drug release per hour per HA-NP,  $\beta$ . The estimated values of rate constants obtained from the slopes of curves shown in Fig 5 are given in Table 3. In general, a  $\varphi=1$  suggests that drug release and polymer degradation rate are equal. When  $\varphi>1$ , drug release rate is faster than polymer degradation rate. Otherwise, polymer degradation is predominant. Here, the enzyme or stimuli action on the substrate polymer (HA) does not make a significant change on the value of  $\varphi$  (Table 3). In both cases, the value of  $\varphi$  is greater than 1 with approximately equal values ( $\varphi=1.6$  in the presence and  $\varphi=1.5$  in the absence of enzyme).

In each case, the HA-NP degradation rate is significantly higher in the presence of HAase enzyme (median  $\alpha=0.0163$  per h) than in the absence of HAase enzyme (median  $\alpha=0.0044$  per h) indicating 3.7 fold difference between both conditions. The nanocarrier degradation rate constant is fundamentally related to the physicochemical properties of the nanocarrier matrix. In this study, the hyaluronic acid nanocarrier is a well-known substrate of the enzyme hyaluronidase [27]. According to Drugbank, hyaluronic acid (with logP= -6.62, watersolubility= 5 mg/ml, pka=3-4, with a formula structure =  $C_{28}H_{44}N_2O_{23}$ ) is an anionic, nonsulfated glycosaminoglycan naturally found in connective, epithelial, and neural tissues. It is reasonably speculated that this specific rate constant would be lower in aqueous media for a hydrophobic nanocarrier or a nanocarrier that is not a bioactive enzyme substrate. However, there is only a nominal effect on the rate of drug release per nanoparticle (median  $\beta=0.64$  per nanoparticle in the presence of HAase enzyme and median  $\beta=0.60$  per nanoparticle in the absence of HAase enzyme). The intrisinsic drug release rate constant per nanocarrier remained essentially the same in both

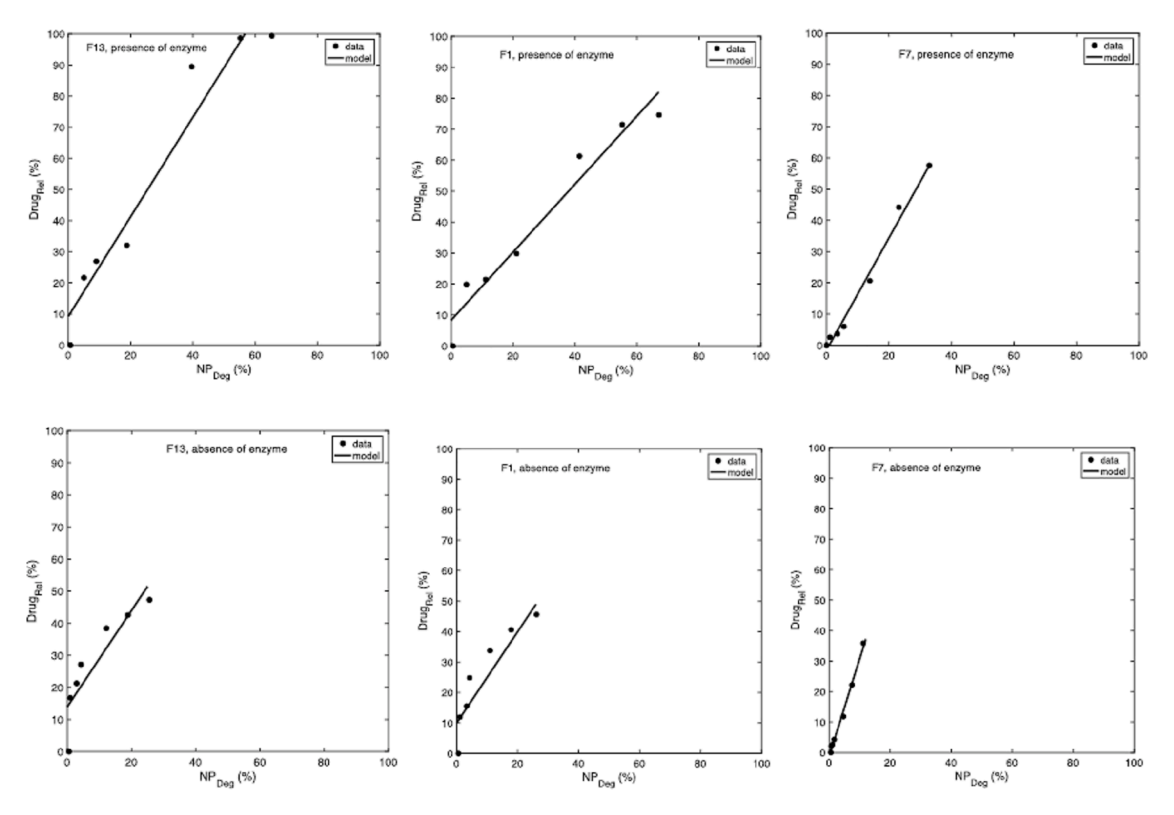


Fig. 5. The prediction of the model (Eq. (11)) (solid line) to the experimental data (filled circle) containing drug release versus HA-NP degradation.

Table 3 Estimated rates of HA-NP degradation,  $\alpha$ , the rate of drug release per HA-NP,  $\beta$ , the net effect,  $\gamma$ , and the drug-controlled release index,  $\phi$ , for cases with and without HAase enzyme.

NPs (Size, nm)	With Enzymes			Without Enzymes				
	α (#NP/ hr)	β (Drug Amount/ NP)	γ (Drug Amount released/ hr)	φ	α (#NP/ hr)	β (Drug Amount/ NP)	γ (Drug Amount released/ hr)	φ
F13 (70.6)	0.0163	0.64	0.0104	1.6	0.0047	0.60	0.0028	1.5
F1 (81.5)	0.0172	0.44	0.0076	1.1	0.0044	0.60	0.0026	1.5
F7 (157.7)	0.0064	0.72	0.0046	1.8	0.0016	1.29	0.0021	3.2
Median:	0.0163	0.64	0.0076	1.6	0.0044	0.60	0.0026	1.5

conditions because it fundamentally depended on the intrinsic physicochemical property of the drug under consideration instead. For tenofovir (TFV), this factor depends on its water solubility, logP, pka, molecular weight (MW), etc.... In fact, according to Drugbank, TFV molecule [with a formula structure =:  $C_9H_14N_5O_4P$ , MW: 287.2123, melting point = 279 °C, pka (strongest acid)= 1.35, pka (strongest basic) = 3.74, physiological charge= - J is a biopharmaceutic classification system (BCS) class 3 drug due to its high aqueous solubility (1.87 mg/mL) and low permeability [53]. It is reasonably speculated that this second rate constant would be lower for a hydrophobic drug substance in an aqueous media.

Hence, our results show that more TFV is available in the presence of HAase enzyme due to higher degradation of HA-NPs in the presence of enzyme rather than due to higher amount of drug released per HA-NP.

Using per capita rate constant  $\alpha$  (#NP per hr) and  $\beta$  (amount of drug released per NP), the net effect,  $\gamma$  (amount of drug released per hr), of the release condition on the nanomedicine is defined as follows:

$$\gamma = \alpha \beta$$
. (12)

The estimated values of rate constants are given in Table 3. In each case, the net effect is significantly higher in the presence of HAase enzyme (median  $\gamma=0.0028$  per h) indicating 2.9 fold difference between conditions with presence and absence of HAase enzyme. As a result of a higher net effect, the total amount of free drug available is significantly higher in the presence of HAase enzyme (Fig. 6). Among HA-NP used in this study, the maximum free drug release is faster in F13, followed by F1 and then by F7 (Fig. 6) mainly due to their difference in size and specific surface area. Overall, the F13 appears to be the best stimuli-sensitive release NMs based on the highest value of the "phi" ratio obtained after enzyme exposure (1.6) vs without the enzyme (1.5). For F1 and F7, the drug release rate constant was relatively higher without the enzyme, perhaps due to poor drug entrapment, higher matrix porosity/cross linking density in larger size particles.

# 4. Conclusion

This study capitalized on a deterministic approach to modelling a HIV/AIDS microbicide, Tenofovir release kinetics from hyal-uronidase-sensitive nanomedicine (NM) or nanoparticle (NP). Our model, based on a system of two differential equations (accounting for NM degradation and then drug release from degraded NM), enabled to estimate the per capita rate constant  $\alpha$  (#NP/hr) and  $\beta$  (Drug Amount Released/NP), the net effect of the NM (NE factor  $\gamma = \alpha \beta$ ) and the controlled index ( $\phi$ , ratio of drug release to NP degradation enabling to select the best stimuli-sensitive NMs during formulation screening). The model analysis conducted with tenofovir loaded hyaluronidase sensitive NM clearly shows the  $\alpha$  factor significantly increased with triggering stimuli due to its enzymatic action on substrate (hyaluronic acid). However, the  $\beta$  factor remained relatively unchanged, due to intrinsic physicochemical properties of the drug as limiting factor. This unique approach is applicable for a more specific and more meaningful/physicochemically relevant description of bioactive agent release from NM or NPs for various applications. This deterministic approach to NM study could potentially impact particle dosimetry, particokinetic and nanotoxicity for safe and effective NM.

We acknowledge some limitations of our study. Our modeling approach is based on the assumption that deterministic and stochastic events might have some role in NPs degradation and drug release. However, given the large number of NPs, we expect to have the less impact of stochasticity. The diffusion coefficient in various media are estimated from Stokes-Einstein's equation. More accurate estimates of the diffusion coefficients, including effects of hindered motion if any, can help improve our results. The particles number are estimated based on equation assuming that particles are assimilated to sphere. An accurate experimental measurement counting of each particle could allow to refine the model. In this study, the polymeric matrix degradation is considered as NPs degradation measured by biochemical method instead of more accurate methods such as size exclusion, size exclusion chromatography. For simplicity and proof of concept, we have also ignored the thermodynamics aspects of these complex nanosystems.

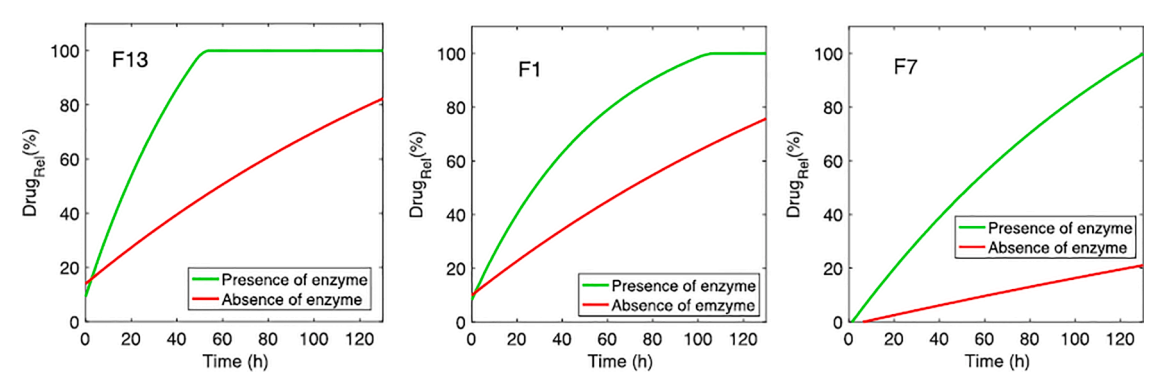


Fig. 6. The prediction of the model for drug release over time in the presence (green) and absence (red) of HAase enzyme.

# CRediT authorship contribution statement

Coulibably contributed to the collection of the experimental data and writing. Vivek Agrahari contributed in the manufacturing and characterization of HA-NPs and writing of this manuscript.

Naveen Vaidya performed the mathematical modeling and writing of the mathematical sections.

Bi-Botti C. Youan performed writing, the original draft and conceptualization.

# **Declaration of Competing Interest**

The authors declare no conflict of interest.

#### Acknowledgment

The work of NKV was partially supported by NSF grants DMS-1951793, DMS-1836647, and DEB-2030479 from the National Science Foundation of USA, and the UGP award from San Diego State University. The project was supported by Award Number R01AI087304 from the National Institute of Allergy and Infectious Diseases (Bethesda, MD, USA). The content is the sole responsibility of the authors and does not necessarily represent the official views of the National Institute of Allergy and Infectious Diseases or the National Institutes of Health

# References

- [1] A. Bowen, E.E. Sweeney, R. Fernandes, Nanoparticle-based immunoengineered approaches for combating HIV, Front. Immunol. (2020) 11.
- [2] M.A. Macchione, D. Aristizabal Bedoya, F.N. Figueroa, M. Muñoz-Fernández, M.C Strumia, Nanosystems applied to HIV infection: prevention and treatments, Int. J. Mol. Sci. 21 (22) (2020).
- [3] T. Mamo, E.A. Moseman, N. Kolishetti, C. Salvador-Morales, J. Shi, D.R. Kuritzkes, et al., Emerging nanotechnology approaches for HIV/AIDS treatment and prevention, Nanomedicine 5 (2) (2010) 269–285 (Lond).
- [4] V.B. Oti, Nanoparticles and Its implications in HIV/AIDS therapy, Curr. Drug Discov. Technol. 17 (4) (2020) 448-456.
- [5] S.K. Lai, Y.Y. Wang, J. Hanes, Mucus-penetrating nanoparticles for drug and gene delivery to mucosal tissues, Adv. Drug Deliv. Rev. 61 (2) (2009) 158-171.
- [6] Y.Y. Wang, S.K. Lai, C. So, C. Schneider, R. Cone, J. Hanes, Mucoadhesive nanoparticles may disrupt the protective human mucus barrier by altering its microstructure, PLoS One 6 (6) (2011) e21547.
- [7] L.M. Ensign, C. Schneider, J.S. Suk, R. Cone, J. Hanes, Mucus penetrating nanoparticles: biophysical tool and method of drug and gene delivery, Adv. Mater. 24 (28) (2012) 3887–3894.
- [8] S.K. Lai, K. Hida, S. Shukair, Y.Y. Wang, A. Figueiredo, R. Cone, et al., Human immunodeficiency virus type 1 is trapped by acidic but not by neutralized human cervicovaginal mucus, J. Virol. 83 (21) (2009) 11196–11200.
- [9] Y. Cu, W.M. Saltzman, Controlled surface modification with poly(ethylene)glycol enhances diffusion of PLGA nanoparticles in human cervical mucus, Mol. Pharm. 6 (1) (2009) 173–181.
- [10] L.M. Ensign, B.C. Tang, Y.Y. Wang, T.A. Tse, T. Hoen, R. Cone, et al., Mucus-penetrating nanoparticles for vaginal drug delivery protect against herpes simplex virus. Sci. Transl. Med. 4 (138) (2012) 138ra79.
- [11] E.J. Oh, K. Park, K.S. Kim, J. Kim, J.A. Yang, J.H. Kong, et al., Target specific and long-acting delivery of protein, peptide, and nucleotide therapeutics using hyaluronic acid derivatives, J. Control. Release 141 (1) (2010) 2–12.
- [12] G.I. Swyer, The hyaluronidase content of semen, Biochem. J. 41 (3) (1947) 409–413.
- [13] V. Agrahari, C. Zhang, T. Zhang, W. Li, T.K. Gounev, N.A. Oyler, et al., Hyaluronidase-sensitive nanoparticle templates for triggered release of HIV/AIDS microbicide in vitro, AAPS J. 16 (2) (2014) 181–193.
- [14] A. Hadjitheodorou, G. Kalosakas, Analytical and numerical study of diffusion-controlled drug release from composite spherical matrices, Mater. Sci. Eng. C 42 (2014) 681–690. Materials for biological applications.
- [15] D. Klose, F. Siepmann, K. Elkharraz, J. Siepmann, PLGA-based drug delivery systems: importance of the type of drug and device geometry, Int. J. Pharm. 354 (1–2) (2008) 95–103.
- [16] J. Siepmann, F. Lecomte, R. Bodmeier, Diffusion-controlled drug delivery systems: calculation of the required composition to achieve desired release profiles, J. Control. Release 60 (2–3) (1999) 379–389.
- [17] C.M.L. FGJP, H.E. Junginger, J.J. Tukker, An estimate of turnover time of intestinal mucus gel layer in the rat in situ loop, Int. J. Pharm. 70 (3) (1991) 235–240.
- [18] Y. Fu, W.J. Kao, Drug release kinetics and transport mechanisms of non-degradable and degradable polymeric delivery systems, Expert Opin. Drug Deliv. 7 (4) (2010) 429–444.
- [19] P. Costa, J.M. Sousa Lobo, Modeling and comparison of dissolution profiles, Eur. J. Pharm. Sci. 13 (2) (2001) 123-133.

[20] S.K. Lai, D.E. O'Hanlon, S. Harrold, S.T. Man, Y.Y. Wang, R. Cone, et al., Rapid transport of large polymeric nanoparticles in fresh undiluted human mucus, Proc. Natl. Acad. Sci. U. S. A. 104 (5) (2007) 1482–1487.

- [21] J.K. MG, U.F. Schaefer, M. Schneider, C.M. Lehr, Computational fluid dynamics of nanoparticle disposition in the airways: mucus interactions and mucociliary clearance, Comput. Vis. Sci. (14) (2011) 301–308.
- [22] V. Agrahari, B.B. Youan, Sensitive and rapid HPLC quantification of tenofovir from hyaluronic acid-based nanomedicine, AAPS PharmSciTech. 13 (1) (2012) 202–210
- [23] F.S. Coulibaly, M.J.M. Ezoulin, S.S. Purohit, N.J. Ayon, N.A. Oyler, B.C. Youan, Layer-by-Layer Engineered Microbicide Drug Delivery System Targeting HIV-1 gp120: physicochemical and Biological Properties, Mol Pharm 14 (10) (2017) 3512–3527.
- [24] D.H. Owen, D.F. Katz, A vaginal fluid simulant, Contraception 59 (2) (1999) 91–95.
- [25] D.H. Owen, D.F. Katz, A review of the physical and chemical properties of human semen and the formulation of a semen simulant, J. Androl. 26 (4) (2005) 459–469.
- [26] I. Youm, V. Agrahari, J.B. Murowchick, B.B. Youan, Uptake and cytotoxicity of docetaxel-loaded hyaluronic acid-grafted oily core nanocapsules in MDA-MB 231 cancer cells, Pharm. Res. 31 (9) (2014) 2439–2452.
- [27] V. Agrahari, C. Zhang, T. Zhang, W. Li, T.K. Gounev, N.A. Oyler, et al., Hyaluronidase-sensitive nanoparticle templates for triggered release of HIV/AIDS microbicide in vitro, AAPS J. 16 (2) (2014) 181–193.
- [28] T. BITTER, H.M MUIR, A modified uronic acid carbazole reaction, Anal. Biochem. 4 (1962) 330-334.
- [29] B. Jachimska, A. Pajor, Physico-chemical characterization of bovine serum albumin in solution and as deposited on surfaces, Bioelectrochemistry 87 (2012) 138–146.
- [30] H.T. Phan, S. Bartelt-Hunt, K.B. Rodenhausen, M. Schubert, J.C. Bartz, Investigation of bovine serum albumin (BSA) attachment onto self-assembled monolayers (SAMs) using combinatorial quartz crystal microbalance with dissipation (QCM-D) and spectroscopic ellipsometry (SE), PLoS One 10 (10) (2015), e0141282.
- [31] S. Sasaki, Y. Iida, Effects of the kinematic viscosity and surface tension on the bubble take-off period in a catalase-hydrogen peroxide system, Colloids Surf. B Biointerfaces 71 (1) (2009) 124–127.
- [32] A. Einstein, Über die von der molekularkinetischen theorie der wärme geforderte bewegung von in ruhenden flüssigkeiten suspendierten Teilchen, Ann. Phys. 322 (1905) 549–560.
- [33] S. Mv, Zur kinetischen theorie der brownschen molekularbewegung und der suspensionen, Ann. Phys. 326 (14) (1906) 756-780.
- [34] O. Annunziata, D. Buzatu, J.G. Albright, Protein diffusion coefficients determined by macroscopic-gradient Rayleigh interferometry and dynamic light scattering, Langmuir 21 (26) (2005) 12085–12089.
- [35] S. Li, D. Xing, J. Li, Dynamic light scattering application to study protein interactions in electrolyte solutions, J. Biol. Phys. 30 (4) (2004) 313-324.
- [36] J. Stetefeld, S.A. McKenna, T.R. Patel, Dynamic light scattering: a practical guide and applications in biomedical sciences, Biophys. Rev. 8 (4) (2016) 409-427.
- [37] N.F. Britton, Essential Mathematical Biology, Springer-Verlag London, 2003.
- [38] Y. Gao, D.F. Katz, Multicompartmental pharmacokinetic model of tenofovir delivery by a vaginal gel, PLoS One 8 (9) (2013) e74404.
- [39] B.E. Lai, M.H. Henderson, J.J. Peters, D.K. Walmer, D.F. Katz, Transport theory for HIV diffusion through in vivo distributions of topical microbicide gels, Biophys. J. 97 (9) (2009) 2379–2387.
- [40] P. Snetkov, K. Zakharova, S. Morozkina, R. Olekhnovich, M. Uspenskaya, Hyaluronic acid: the influence of molecular weight on structural, physical, physicochemical, and degradable properties of biopolymer, Polymers 12 (8) (2020) (Basel).
- [41] S.U. Choi, T. Bui, R.J. Ho, pH-dependent interactions of indinavir and lipids in nanoparticles and their ability to entrap a solute, J. Pharm. Sci. 97 (2) (2008) 931–943.
- [42] I. Ocao, Density, viscosity and refractive index of the dimethyl sulfoxide + o-xylene system, J. Serb. Chem. Soc. 74 (3) (2009) 317-329.
- [43] I. OCaO, Vapor pressure, density, viscosity and refractive index of dimethyl sulfoxide + 1,4-dimethylbenzene system, J. Serb. Chem. Soc. 73 (1) (2008) 73–85.
- [44] X. Wang, G. Herting, I.O. Wallinder, E. Blomberg, Adsorption of bovine serum albumin on silver surfaces enhances the release of silver at pH neutral conditions, Phys. Chem. Chem. Phys. 17 (28) (2015) 18524–18534.
- [45] T. Kongraksawech PV-L, J. Huerta-Ruelas, J. A, Torres Ionic strength and pH effects on optical thermographs for bovine serum albumin (BSA), Cienc. Tecnol. Aliment. 5 (4) (2007) 259–264.
- [46] S. Ge, K. Kojio, A. Takahara, T. Kajiyama, Bovine serum albumin adsorption onto immobilized organotrichlorosilane surface: influence of the phase separation on protein adsorption patterns, J. Biomater. Sci. Polym. Ed. 9 (2) (1998) 131–150.
- [47] R. Li, Z. Wu, Y. Wangb, L. Ding, Y. Wang, Role of pH-induced structural change in protein aggregation in foam fractionation of bovine serum albumin, Biotechnol. Rep. 9 (2016) 46–52 (Amst).
- [48] S.P. Boulos, T.A. Davis, J.A. Yang, S.E. Lohse, A.M. Alkilany, L.A. Holland, et al., Nanoparticle-protein interactions: a thermodynamic and kinetic study of the adsorption of bovine serum albumin to gold nanoparticle surfaces, Langmuir 29 (48) (2013) 14984–14996.
- [49] B. AK, Adsorption of bovine serum albumin onto glass powder surfaces coated with polyvinyl alcohol, J. Appl. Polym. Sci. 78 (5) (2000) 933–940.
- [50] S. Servagent-Noinville, M. Revault, H. Quiquampoix, M. Baron, Conformational changes of bovine serum albumin induced by adsorption on different clay surfaces: FTIR analysis, J. Colloid Interface Sci. 221 (2) (2000) 273–283.
- [51] J. Waniewski, Mean transit time and mean residence time for linear diffusion–convection–reaction transport system, Comput. Math. Methods Med. 8 (1) (2007) 37-49
- [52] K.H. Ramteke, P.A. Dighe, A.R. Kharat, S.V. P. Mathematical models of drug dissolution: a review, Sch. Acad. J. Pharm. 3 (2014) 388-396.
- [53] A.N. Ngo, M.J. Ezoulin, J.B. Murowchick, A.D. Gounev, B.B. Youan, Sodium acetate coated tenofovir-loaded chitosan nanoparticles for improved physico-chemical properties, Pharm. Res. 33 (2) (2016) 367–383.